Surface Structure of $(10\bar{1}0)$ and $(11\bar{2}0)$ Surfaces of ZnO with Density Functional Theory and Atomistic Simulation

David J. Cooke, Arnaud Marmier, and Stephen C. Parker*

Department of Chemistry, University of Bath, BATH, United Kingdom

Received: November 8, 2005; In Final Form: January 20, 2006

We have calculated the stability of two of the low-index surfaces known to dominate the morphology of ZnO as a function of stoichiometry. These two surfaces are $(10\bar{1}0)$ and $(11\bar{2}0)$. In each case, two terminations only are stable for a significant range of oxygen and hydrogen chemical potential: the pure stoichiometric surface and a surface covered in a monolayer of water. The mode by which the water adsorbs is however different for the two surfaces considered. On the $(10\bar{1}0)$ surface the close proximity of the water molecules means hydrogen bonding can occur between adjacent chemiabsorbed water molecules and hence there is little difference in the stability of the hydrated and hydroxylated surface, and in fact the most stable surface occurs with a combination of dissociated and undissociated water adsorption. In the case of the $(11\bar{2}0)$ surface, it is only when full dissociation has occurred that a hydrogen-bonding network can form. Our results also show good agreement between DFT and atomistic simulations, suggesting that potential based methods can usefully be applied to ZnO.

1. Introduction

The aim of this work is to calculate the surface structure and composition of the important nonpolar, low-index surfaces of ZnO. The surface structure of ZnO is of particular interest because the chemical properties of ZnO lie on the borderline between ionic and covalent solids[1,2] and consequently the material has a wide range of technical uses including as a catalyst and a sensor material.[3]

An understanding of these important processes requires a detailed knowledge of the variation of surface structure and stability under a variety of different conditions, particularly as a function of O_2 and H_2 partial pressure. The potentially complex defect chemistry of ZnO is exemplified by the color changes with oxygen content. Stoichiometric ZnO is a white solid with the wurtzite structure but on heating the color changes to yellow due to the evaporation of oxygen from the lattice to give a nonstoichiometric structure containing oxygen vacancies and trapped electrons which can be excited by the adsorption of visible light.[4] Indeed oxygen vacancies are known to be the most common form of defect in bulk ZnO.[5] The maximum deviation from stoichiometry for this color change to occur is small (zinc excess <70 ppm); however, by doping the material with a higher concentration of zinc (0.02−0.03%) a range of colors from green to red/brown can be obtained.[6]

Four low-index surfaces dominate the morphology of ZnO, namely the nonpolar $(10\bar{1}0)$ and $(11\bar{2}0)$ surfaces, along with the polar (0001)-Zn and $(000\bar{1})$-O surfaces. All four surfaces have previously been studied experimentally[2,7] and a detailed theoretical study of the stoichiometric surfaces of ZnO has been performed by Meyer and Marx.[8]

The work described in this paper aims to go beyond the simple stoichiometric systems by considering the effect of nonstoichiometry, and hence evaluate the optimum composition of the surface under different external conditions, making the calculations more comparable to experiment. The approach is to compute the surface energy of defective and nonstoichiometric oxide surfaces in equilibrium both with their bulk structure and with an atmosphere of gases at various temperatures and partial pressures. This technique provides a good understanding of surface structure and stability under different conditions, whether ultrahigh vacuum, low temperature, or a natural environment. Although the idea of using chemical potential to treat defects is not new, the explicit linking with partial pressures using experimental tabulated data is relatively recent and has been popularized for nonstoichiometric oxide surfaces by the groups of Sheffler[9,10] and Finnis.[11] We have already successfully applied this methodology to the low-index surfaces of alumina (α-Al_2O_3)[12,13] and others have used a similar approach to study the (0001)[14,15] and $(10\bar{1}0)$[16] surfaces of ZnO. One of the features of most of the published work is that all the thermal contributions to the solid phases are neglected, because these terms are small and computationally expensive to evaluate. We therefore report our recent work based on the two nonpolar surfaces, namely the $(10\bar{1}0)$ and $(11\bar{2}0)$ terminations, using a new alternative approach for calculating the solid thermal contributions of the solid phases. Prior to discussing the results, we outline briefly the underlying methodology and theory.

2. Methodology and Theory

We have used the VASP code (Vienna ab initio simulation package)[17−20] employing Vanderbilt pseudopotentials[21] developed by Kresse and Hafner,[22] which allows a smaller basis set for a given accuracy. Within the pseudopotential approach, only the valence electrons are treated explicitly. The functional was based on the Ceperley−Alder parametrization of the local density approximation.

Initially the experimental bulk crystal is minimized at constant pressure for various sized k-point grids and energy cutoffs to establish the optimum size for these parameters. Once this has

* Address correspondence to this author. E-mail: s.c.parker@bath.ac.uk.

10.1021/jp0564445 CCC: $30.25
Published on Web 03/29/2006

been achieved, the results can be compared to previous experimental and theoretical studies. In addition, it may also be convenient to compare the calculated bulk properties to those from atomistic calculations based on the Born model of solids.[23]

Surfaces are generated by orientating and cutting the structure to expose the appropriate surface termination. Where a number of terminations are possible it is important to consider all nonequivalent reconstructions. Energy minimization is performed by generating slabs separated by a vacuum gap, and the thickness of the slab and the depth of the vacuum gap must be chosen so they are large enough to prevent interaction between adjacent surfaces when 3D boundary conditions are applied. The appropriate sizes are determined by optimizing the stoichiometric structure for systems of various sizes until convergence in the calculated surface energy is reached. The composition of this optimized system is then perturbed to generate several nonstoichiometric systems.

If it is assumed that ZnO is in chemical equilibrium with an atmosphere containing O_2, H_2, or H_2O, then the oxide slab contains N_{Zn} metal atoms at chemical potential μ°_{Zn}, N_O oxygen atoms at chemical potential μ°_O, and N_H hydrogen atoms at chemical potential μ°_H, and the surface energy can be expressed in terms of these quantities.

Thus the free energy of slabs of different stoichiometry can be used to build up a phase diagram in terms of (μ_O, μ_H) and (T, p_{O_2}, p_{H_2}, p_{H_2O}). A more formal description of the underlying theory used can be found elsewhere;[12] however, it should be noted that one major assumption made in previous studies is that entropic excess contributions to the free energy are negligible. In many solid systems, the zero-point energy will make up a significant contribution to the system and thus it would be desirable to include the vibrational component of free energy in our model.

One approach for calculating the vibrational contribution to the free energy of solids is to use the lattice dynamics approach described by Born and Huang.[23] The technique assumes the vibrational modes are quantized harmonic oscillators, which depend on volume; this is the well-known quasiharmonic approximation. The vibrational frequencies are calculated by first diagonalizing the dynamical matrix, at sufficient points in k-space, and then applying simple statistical mechanical expressions to obtain the thermodynamic properties of the system. The problem with direct calculation of the vibrational frequencies at many points in k-space is that it is computationally expensive. Thus, we propose an alternative, which is to use an interatomic potential model to calculate the vibrational frequencies. There is of course a requirement that the potential model reproduces the dynamical properties. However, in the case of ZnO there are already reliable interatomic potentials available.[24,25] We have followed this method and have successfully modeled the structure and thermodynamic properties of bulk minerals[26,27] and others have applied this technique to modeling defects.[28,29] The approach depends for its success on the assumption that the intrinsic anharmonic contribution to the free energy is negligible, although at ambient temperatures the zero-point energy is going to be much more significant than the intrinsic anharmonic contribution to the vibrational entropy.[30] Assuming this is the case provides a fast and straightforward method for estimating the magnitude of the previously neglected vibrational terms.

3. Results and Discussion

3.1. The Bulk Structure. The experimental structure used as the starting point for this work was that reported by Sawada and co-workers[31] and had unit cell parameters of $a = b = 3.2490$ Å, $c = 5.2052$ Å, $\alpha = \beta = 90°$, and $\gamma = 120°$. The system was then optimized at constant pressure by using the VASP code leading to a crystal structure of $a = b = 3.1959$ Å, $c = 5.1585$ Å, $\alpha = \beta = 90°$, and $\gamma = 120°$. For this calculation, it was found that a cutoff of 500 eV and a k-point grid of $5 \times 5 \times 5$ were sufficient to ensure convergence. The result can be compared with the complementary atomistic approach wth the potential parameters of Nyberg et al.[25] where the cell relaxed such that $a = b = 3.231$ Å, $c = 5.076$ Å, $\alpha = \beta = 90°$, and $\gamma = 120°$ and the potential parameters of Binks[24] where the cell relaxed such that $a = b = 3.271$ Å, $c = 5.138$ Å, $\alpha = \beta = 90°$, and $\gamma = 120°$. While these values differ, it should be noted that the atomistic parameters were fitted to the volume of the structure. The DFT calculation reproduces the c/a ratio of the experimental data to within 0.01 units and the calculated cell parameters are in good agreement with those calculated by Jaffe et al. using a Hartree−Fock approach.[32] The calculated density of states for the bulk structure (not shown) is in good agreement with that previously calculated by Schröer et al.[33] where many of the key features described are readily identifiable. Examples of this include the peak at approximately −16 eV, which corresponds to the s states of the O atoms, with the next peaks at ca. −5 eV corresponding to the O 2p states and the remaining peaks Zn 3d states.

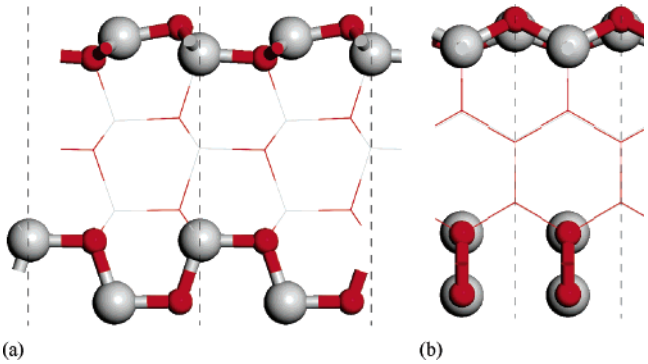

Figure 1. The relaxed structure of the two possible terminations of the ZnO ($10\bar{1}0$) surface. At the top the closed structure and at the bottom the open structure (side views). The large light gray sphere represents Zn, the small dark gray sphere represents O.

3.2. The ($10\bar{1}0$) Surfaces. The terminations of the ($10\bar{1}0$) surface were modeled by using a slab of six repeat distances thick, which corresponds to a depth of 20 Å. A vacuum gap of a further 20 Å was sufficient to ensure there was no interaction between adjacent slabs and between the surfaces at the top and bottom of the slab, which are identical. This resulted in a slab of surface area 3.20×5.16 Å^2 and containing 24 ions (in the stoichiometric case). We also performed additional calculations with (2×1) and (2×2) supercells (containing 48 and 96 atoms, respectively) to explore domains of lower "defect" concentration.

3.2.1. Stoichiometric Surfaces. We identified two potentially stable, stoichiometric surface terminations. These systems are illustrated in Figure 1 where (2×2) structures are shown. In both cases, the surface consists of layers of zinc and oxygen. Half the atoms are below the uppermost atoms in the layer. These atoms act as bridges and maintain a coordination of four (equivalent to that of the bulk cell), while the uppermost ions only have a coordination of three. The main difference between the two most stable surface terminations relates to the position of the bridging ions. When the bridging ions are 0.92 Å below the uppermost atoms, a flat (closed) surface termination results. Whereas when the bridging atoms are 1.84 Å below the surface the resulting surface has a far more open, facetted structure.

TABLE 1: Composition (N_{Zn},N_O,N_H) and Energy (in eV) of the 18 Slabs Considered for the (1010) Surface

surface type	coverage (%)	composition	slab energy (closed)	slab energy (open)
stoichiometric		12,12,0	−125.14	−121.54
Zn rich	25	48,46,0	−483.19	
	50	24,22,0	−232.86	
	100	12,10,0	−107.29	−106.45
O rich		10,12,0	−112.71	−112.60
H		12,12,2	−131.86	−131.18
OH + H	50	24,26,6	−282.29	
	100	12,14,4	−156.83	−157.05
H_2O/OH + H		24,28,8	−315.54	
H_2O	50	24,26,4	−282.16	
	100	12,14,4	−157.31	−156.41
	100	24,28,8	−314.65	

On relaxation, the surface energy is calculated as 1.19 J·m^{-2} for the closed surface and 2.94 J·m^{-2} for the open surface.

Previously Wander and Harrison[34] calculated the surface energy of the closed structure using ab initio, all-electron total energy calculations, employing local basis sets, to be 1.16 J·m^{-2}, which is in excellent agreement with our calculated value. Atomistic potential models have also been used to calculate the surface energy at 1.1 J·m^{-2} [25] and 1.00 J·m^{-2},[35] again in good agreement with the DFT results.

Following the energy minimization of the more stable, closed, surface the under coordinated, uppermost, Zn atoms relaxed into the surface by 0.33 Å (0.3 ± 0.15 Å from LEED experiments[36]), whereas the uppermost oxygen atoms only relax by 0.05 Å (0.1 ± 0.05 Å) into the surface. The result of the surface relaxation leads to a shortening of both the Zn−O bond at the surface (from 1.98 Å to 1.83 Å) and, similarly, the Zn−O bond between the Zn and the O in the layer below reduces, in this case form 1.94 Å to 1.89 Å. In the less stable, open surface a similar trend is seen, where the uppermost Zn atoms relax 0.31 Å into the surface during the energy minimization while the uppermost oxygen atoms move out of the surface by 0.11 Å. This again led to a reduction in the Zn−O bond distances of the surface atoms from 1.98 Å and 1.94 Å to 1.74 Å and 1.84 Å, respectively.

The large relaxation of the surface cations has been previously noted by calculations[8,37,38] and is attributed to competition between dihybridization and charge-transfer effects. The success in modeling the stoichiometric surfaces therefore gives us confidence to extend our study to nonstoichiometric surfaces.

The next stage of a thermodynamic study is to calculate the surface energies of various nonstoichiometric surfaces as a function of oxygen and hydrogen chemical potential by using the methodology described previously. The characteristics and energy of the various surfaces investigated are given in Table 1. In each case, we observed that the systems based on the closed structure were more stable.

We have found that the best way to compare the stability of the terminations is to represent the stability domains (i.e., the phase with the lower surface energy) in a phase diagram. While this way of presenting the data loses the value of the surface energies, it gains in clarity. The term phase diagram is slightly confusing though, as not enough surfaces corresponding to intermediate coverages have been calculated and the boundaries between phases are still simplistic. Furthermore, it is always possible that we have missed more stable but more complex surfaces: for instance in the case of (0001), Kresse et al.[15] observe that a combination of triangular vacancy and hydroxyl groups can be more stable in a small domain of their phase diagram.

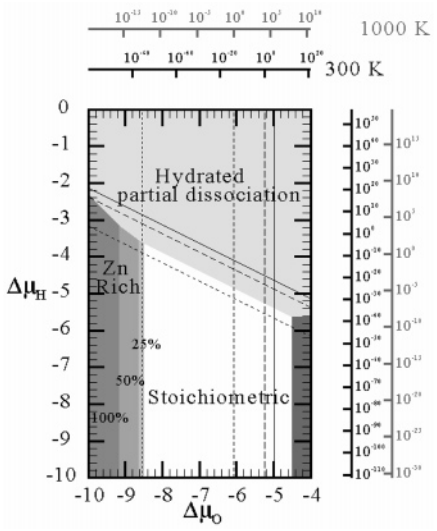

Figure 2. Calculated phase diagram of the structure of the ZnO (10$\bar{1}$0) surface as a function of oxygen and hydrogen chemical potentials or partial pressures. The dotted vertical line on the left-hand side limits the stability domain of solid zincite with respect to metal zinc. The vertical lines on the right-hand side correspond to the condensation of oxygen into molecular O_2, at different temperatures (full 0 K, broken 298 and 1000 K). The diagonal lines correspond to the water/H_2 equilibrium (same temperature convention). The lower and left scales give the chemical potentials, in eV. The upper and right scales give the corresponding partial pressure at 298 and 1000 K, in bar.

TABLE 2: Percentage Vibrational Contribution to the Surface Free Energy of Some of the Most Stable Terminations of the (1010) Surface Relative to the Energy of the System

surface type	0 K (ZPE)	300 K	500 K	700 K	900 K
stoichiometric	−0.96	−0.35	0.80	2.33	4.15
H_2O	−1.66	−1.13	−0.12	1.25	2.87
OH + H	−1.54	−0.94	0.17	1.63	3.37
H_2O/OH + H	−1.58	−1.00	0.07	1.51	3.20
Zn rich (100%)	−1.00	−0.26	1.05	2.77	4.78
Zn rich (50%)	−0.99	−0.34	0.88	2.48	4.37
Zn rich (25%)	−0.97	−0.34	0.85	2.42	4.28
O rich (100%)	−0.91	−0.19	1.08	2.75	4.70

The surface energies used to construct Figure 2 also include the additional vibrational contributions neglected by previous studies. These contributions, as shown in Table 2, are, however, small (typically less than 1% of the total free energy) and thus can safely be neglected in the majority of cases. However, as the temperature increased, such differences become more important. We chose to use the value of the correction at 300 K to plot the phase diagram, and therefore the partial pressure scales are only qualitative.

Keeping in mind the limitation of the phase diagram mentioned above, we discuss the geometric properties of these nonstoichiometric terminations which do appear stable under some reasonable conditions of oxygen and hydrogen chemical potentials.

3.2.2. Zinc-Rich Surfaces. The zinc-rich surfaces were created by removing one uppermost oxygen atom from both faces of 1 × 1, 1 × 2, and 2 × 2 slabs, corresponding to defect coverage of 100%, 50%, and 25%. Our calculations predict that these structures would be observed at low oxygen chemical potential (high temperature and low pressure). Only the 25% oxygen defective surface is stable for a realistic range of chemical potential, i.e., when bulk ZnO is itself stable (to the right of the left-hand vertical broken line). The predicted stability of this type of surface is in line with previous studies discussed

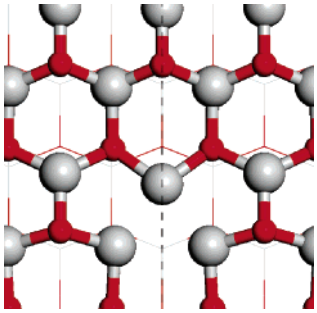

Figure 3. The nonstoichiometric, Zn-rich (25%) $(10\bar{1}0)$ surface, calculated as being stable at high temperature and under ultrahigh vacuum (top view). Same color convention as Figure 1.

above, where on heating some oxygen is lost from the ZnO structure, causing a color change. Due to limitations in computer resources the deviation from stoichiometry in our calculation is far higher than the limit seen experimentally.[4]

There is very little relaxation taking place when one out of four oxygens is removed (see Figure 3). In contrast, when the surface is fully relaxed, the surface becomes practically flat with the zinc atoms previously 0.92 Å above the bridging layer of atoms (in the relaxed stoichiometric structure) relaxing only 0.4 Å above the bridging layer. The reduction in the number of surface oxygen atoms means that the Zn−O bond at the surface is increased to minimize the repulsion between the surface Zn ions. The surface Zn−Zn bond distance is calculated to be 2.59 Å.

3.2.3. Oxygen-Rich Surface. The oxygen-rich surface is calculated to be stable at very high oxygen potentials and is only likely to be observed if kinetically stabilized or by the presence of impurities.

The surface oxygen atoms have undergone considerable relaxation, compared to their position in the relaxed stoichiometric structure. The uppermost oxygen atoms are now 0.75 Å above the uppermost zinc atoms in the complete Zn−O layer below (compared with 0.81 Å in the stoichiometric structure). The surface oxygen atoms remain in 3-fold coordination but are now bonded to only two zinc atoms and an oxygen atom from the layer below. The O−O bond length is 1.53 Å, whereas the two Zn−O bonds are 2.06 and 2.10 Å, similar to that found in zinc peroxide, both experimentally[39,40] and when the bulk structure of ZnO_2 is relaxed at constant pressure using the same pseudopotentials as we used for ZnO. Despite this relaxation, the oxygen-rich termination is still stepped compared with the zinc-rich surfaces, and this goes some way to explaining why it is far less stable and why we do not predict that this surface will form in preference to the stoichiometric surface.

3.2.4. Hydrated Surfaces. In natural samples, water is ubiquitous and thus the surfaces are likely to be hydrated. Water can adsorb associatively and disassociatively.

When the primitive cell is considered (i.e., 100% coverage and by periodicity all the water molecule are the same), it is the associative adsorption of the molecular water to this surface that is energetically favored. We do, however, note that the calculated energy of both models of adsorption is similar and therefore expect that when considering different concentrations of water the hydroxylated system may become more stable. We also note that the calculated difference in energy between the two systems (0.24 eV/water) is similar to the difference between the hydration energy and the hydroxylation energy at 100% coverage calculated using atomistic simulations and static, energy minimization (0.44 eV/water). The potential based calculations also do suggest that there would be a preference

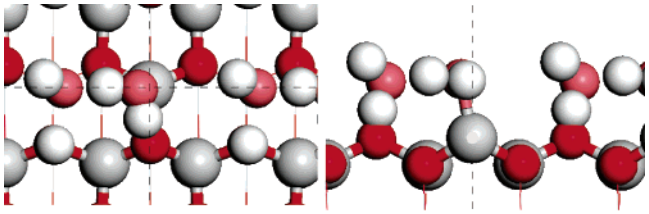

Figure 4. The most stable hydrated structure for the $(10\bar{1}0)$ surface, where partial dissociation is in evidence: (a) top view and (b) side view. Same color convention as Figure 1. Additionally, the small medium gray sphere represents the oxygen from the water molecule, and the small white sphere their hydrogens.

for molecular water to be present, even at lower coverages of water. Following minimization, the oxygen atom on the water molecule has moved away from the surface to 2.03 Å above the surface zinc atom and has moved in the plane parallel to the surface so the $Zn-O_{water}$ bond is 2.08 Å. This movement, together with the rotation of the hydrogen atoms so they are angled toward the surface suggests that the surface is stabilized by hydrogen bonding between the hydrogen atoms and surface oxygen atoms. This $O_{surface}-H$ bond distance of 1.53 Å is equivalent to a short hydrogen bond and hence strongly bound. Such a configuration may also be an indication that there is only a small energy to be overcome before dissociation will occur.

The less stable hydroxylated surface has a structure that is remarkably similar to that described above, thus accounting for the similarities in the calculated energy, the bond distance $O_{surface}-H$ is now only 1 Å, since dissociation has occurred but the bond distance between the hydroxide oxygen and this hydrogen is only 1.52 Å. The surface has also undergone some reconstruction such that the $Zn-O_{hydroxide}$ bond distance is 1.83 Å, significantly shorter than calculated for molecular water.

When a larger cell is considered (2×1), a more complex picture appears as a combination of one dissociated and one undissociated water molecule is even more stable than two undissociated water molecules, and this by 0.22 eV/water. The relaxed surface is shown in Figure 4. The distances between the two O_{water} and the Zn atoms they are adsorbed upon are 1.99 and 1.89 Å for the undissociated and dissociated molecules, respectively. The captured proton sits at a distance of 0.99 Å from the surface oxygen and is separated from its parent hydroxide by 2.11 Å. The physisorbed water molecule is almost flat on the surface, and one of its hydrogen atoms forms a very short hydrogen bond (1.44 Å) with the chemisorbed hydroxide group. While at first surprising, partial dissociation of water is not unknown and has been well documented on MgO.[41,42] More importantly, it has been observed on this same surface by Meyer and co-workers in a recent publication,[16] using experimental probes as well as DFT (GGA-PBE functional). The PBE equilibrium structure is very similar to the LDA one, the only difference being that in the PBE case the water molecules are tilting toward the surface and the proton is exchanged across the trough, while in the LDA case both the tilting and the proton exchange are above the "peak".

3.3. The $(11\bar{2}0)$ Surface. We conclude our discussion by considering the other major nonpolar low-index surface known to dominate the wurtzite structure, namely the $(11\bar{2}0)$ surface. This surface has been less frequently studied than the $(10\bar{1}0)$. Its stoichiometric termination has, however, been the subject of tight binding model studies[43] and ab initio calculations based on DFT (LDA[8] and B3LYP[34]). We have applied the same method as for the $(10\bar{1}0)$ to consider the relative stability of

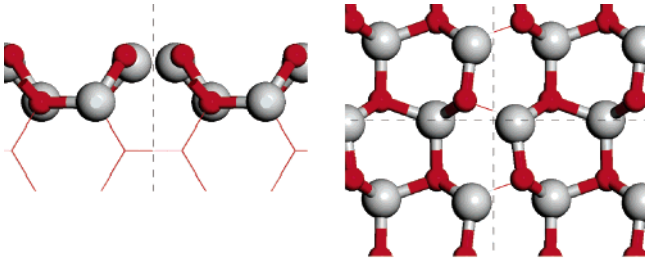

Figure 5. The relaxed structure of the stoichiometric $(10\bar{1}0)$ surface: (a) side and (b) top.

TABLE 3: Composition (N_{Zn},N_O,N_H) and Energy (in eV) of the 16 Slabs Considered for the (1120) Surface

surface type	coverage (%)	composition	slab energy
stoichiometric		10,10,0	−101.84
Zn rich	25 (2 × 1)	20,18,0	−186.40
	25 (1 × 2)	20,18,0	−186.33
	50	10,8,0	−84.49
	100	10,6,0	−65.64
O rich	50	8,10,0	−87.17
	100	6,10,0	−75.81
H	50	10,10,2	−108.17
	100	10,10,4	−114.68
H_2O/OH + H		10,14,8	−167.68
OH + H	50	10,12,4	−133.43
	100	10,14,8	−167.92
H_2O	50	10,12,4	−133.32
	100	10,14,8	−164.50
O rich, H	50	8,10,2	−100.71
	100	8,10,4	−113.23

the stoichiometric surface and deviations from this structure containing varying concentrations of zinc, oxygen, and hydrogen.

The terminations of this surface were modeled by using a slab five repeat distances thick, of surface area 5.21 × 5.63 Å^2 and containing 20 ions (in the stoichiometric case). We also performed additional calculations with (2 × 1) and (1 × 2) supercells to explore lower concentration of defect (down to 25%, as there are already two surface Zn or O for the (1 × 1) cell).

3.3.1. Stoichiometric Surfaces. The stoichiometric surface was generated from the minimized structure in the same way as described for the previous surface. Only one stable termination was identified. Its relaxed structure is shown in Figure 5.

On relaxation the Zn−O bond distance for the surface ions reduces to 1.84 Å whereas the relaxation of the ions in the second layer is much smaller with the Zn−O bond distance being calculated as 1.94 Å both with the surface ions and with those in the same layer. The relaxed surface energy is calculated as 1.23 J·m^{-2}, whereas atomistic simulations calculate the surface energy to be 1.16 J·m^{-2} with use of the potential parameters of Nyberg[25] and 1.20 J·m^{-2} with use of the potential parameters of Binks.[24] Previously Meyer and Marx[8] used local density approximation DFT and calculated the surface energy to be 1.25 J·m^{-2}. Thus, this surface is only slightly less stable than the well-studied $(10\bar{1}0)$ surface.

We next adjusted the amount of surface Zn, O, and H and optimized the structure of each of the configurations described by Table 3. We present the calculated phase diagram in Figure 6, which illustrates the most stable surface composition as a function of hydrogen and oxygen potential. We would like to emphasize that the caveats raised for the $(10\bar{1}0)$ also do apply. Once again, the diagram incorporates the vibrational effects calculated with potential based lattice dynamics. The effect of this term is generally slightly larger than that for $(10\bar{1}0)$, as illustrated in Table 4.

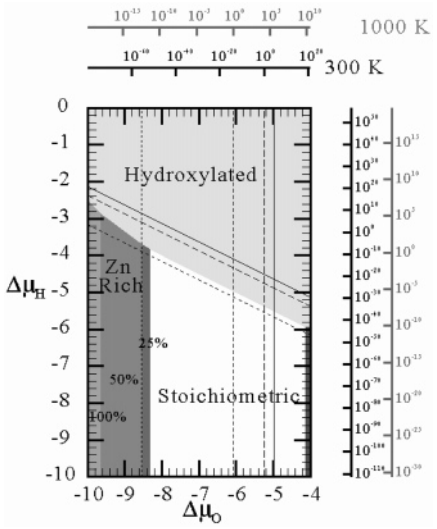

Figure 6. Calculated phase diagram of the structure of the ZnO $(10\bar{1}0)$ surface as a function of oxygen and Hydrogen chemical potentials or partial pressures. Same color conventions as Figure 2.

TABLE 4: Percentage Vibrational Contribution to the Surface Free Energy of Some of the Most Stable Terminations of the (11$\bar{2}$0) Surface Relative to the Energy of the System

surface type	0 K (ZPE)	300 K	500 K	700 K	900 K
stoichiometric	−1.36	−0.47	1.21	3.43	6.06
OH + H (100%)	−2.33	−1.56	−0.20	1.60	3.71
OH + H (50%)	−1.97	−1.14	0.36	2.35	4.69
Zn rich (100%)	−1.69	−0.47	1.71	4.57	7.92
Zn rich (50%)	−0.94	−0.16	1.20	2.97	5.03
Zn rich (25%)	−0.93	−0.23	1.04	2.71	4.66
O rich (100%)	−2.04	−0.61	1.89	5.17	9.02

3.3.2. Zinc-Rich Surfaces. Zinc-rich surfaces were created by removing 25%, 50%, and 100% of the surface oxygen atoms from both surfaces of the slab. Thanks to the stoichiometry of the $(11\bar{2}0)$ surface it was possible to consider removing 50% and 100% of the surface oxygen atoms with the primitive cell, and 25% from (1 × 2) or (2 × 1) supercells. Just as when considering $(10\bar{1}0)$, our calculations predict that the 50% and 100% structures would be observed at high temperature and low oxygen chemical potentials was it not for the fact that under these conditions ZnO is not stable. At the lower defect concentration of 25%, the surface is stable in domain compatible with the stability of the underlying bulk ZnO.

The structure from which 25% of the surface oxygen atoms have been removed is still similar to that found in the stoichiometric structure. The Zn atoms adjacent to the oxygen vacancy have moved 0.16 Å into the surface and closer to each other (2.40 Å from 2.97 Å).

There is more reconstruction at the surface when 50% of the O is removed. The Zn atom adjacent to the oxygen vacancy has moved 0.3 Å into the surface and has moved perpendicular 0.4 Å to the surface such that the bond distance with the oxygen in the layer below has increased slightly, from 1.93 Å to 1.98 Å, and the Zn−Zn bond distance has decreased from 2.97 Å to 2.60 Å.

Further reconstruction occurs when the remaining surface oxygen atoms are removed causing the Zn−O bond distance to lengthen still further to 2.02 Å compensated by a further reduction of the Zn−Zn bond distance to 1.73 Å.

3.3.3. Oxygen-Rich Surface. In common with the $(10\bar{1}0)$

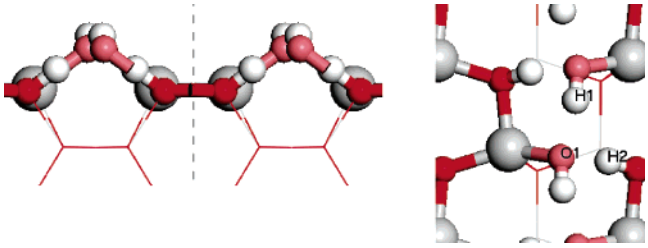

Figure 7. The relaxed structure of the relaxed fully hydroxylated (11.0) surface, illustrating the formation of a hydrogen bonding network on the surface: $H_1-O_1 = 1.77$ Å, $H_2-O_1 = 1.49$ Å.

surface discussed above we predict the oxygen-rich surfaces will only be stable at very high oxygen potentials and therefore only likely to be observed if kinetically stabilized or by the presence of impurities. Systems where 50% and 100% of the surface zinc atoms have been removed were considered.

The structure when 50% of the surface zinc atoms have been removed has undergone a considerable amount of reconstruction in order that each surface oxygen atom remains bonded to one Zn atom with a bond distance equal to that found in the stoichiometric structure. This means the coordination of the surface oxygen atoms reduces from three, in the stoichiometric structure, to two. The reconstruction also extends to the layer immediately below the surface. In the stoichiometric structure the four atoms in this layer are all 1.3 Å below the surface atoms; however, by removing half the surface zinc atoms the atoms below the remaining zinc are now 1.6 Å below the surface whereas below where the surface atom has been removed the gap between this layer and the surface is 1.9 Å.

Removing the remaining zinc atom from the surface causes a change in crystal structure. This is initiated by the surface oxygen atoms relaxing into the layer below. This results in the zinc atoms adopting a square planar coordination, bonded to the two oxygen atoms which have relaxed from the surface, with 2-fold coordination and two bulk oxygen atoms, which are in 4-fold coordination. This effect is exemplified in these five-layer structures because once the oxygen atoms have relaxed into the layer below there is effectively only one bulk layer in the simulation cell.

3.4. Hydrated Surface. We have limited our investigation of the adsorption of water on the $(11\bar{2}0)$ surface to the primitive cell, which already allows us to adsorb two independent water molecules and to generate three configurations: no dissociation, full dissociation, and partial dissociation. At ambient temperatures, we predict that water will be present on the surface. However, unlike in the $(10\bar{1}0)$ surface case, we calculate that the water will form a dissociatively adsorbed layer. We note that the calculated difference in energy between the fully and not at all dissociated systems is quite large (0.85 eV/water). On the other hand, the difference between fully and partially dissociated is very small at 0.06 eV/water and it is possible that on the macro-level both structures will be seen. Calculations using atomistic simulations also predict that the hydroxylated surface is slightly more stable with the difference between hydroxylation and hydration energy being 0.13 eV/water.

The increased stability of the fully hydroxylated surface can be attributed to the formation of a hydrogen bond network on the surface as illustrated in Figure 7 with the hydrogen bond distance calculated as 1.49 and 1.73 Å. Evidence of hydrogen bonding is not seen when a complete layer of molecular water is added to the surface since the adjacent molecules are situated over 2.5 Å apart, hence it is only when dissociation occurs that hydrogen bonding is possible, accounting for the increased stability of the hydroxylated surface.

Additional calculations with atomistic simulation techniques also suggest that 100% coverage represents the most stable concentration of water on the surface, and hence that a complete monolayer is likely to form.

4. Conclusion

We have calculated the stability, as a function of stoichiometry, of two of the low-index surfaces known to dominate the morphology of ZnO. We have considered 18 and 16 different terminations (covering oxygen, hydrogen or water adsorption, zinc and oxygen vacancies) for the $(10\bar{1}0)$ and $(11\bar{2}0)$ surfaces, respectively. The resulting phase diagrams show that at practically all oxygen and hydrogen partial pressures the most stable surface stoichiometry is either the pure stoichiometric surface or a surface covered in a monolayer of water, in contrast to some other surfaces where extensive reconstruction does occur (for instance the (0001)-Zn of ZnO). The mode by which the water adsorbs is, however, different on the two surfaces and is related to the area per water molecule on each surface. On the $(10\bar{1}0)$ surface the close proximity of the water molecules means hydrogen bonding can occur between adjacent chemiabsorbed water molecules meaning there is little difference in the stability of the hydrated and hydroxylated surface. Indeed the most stable surface appears from a combination of dissociated and nondissociated water molecules. In the case of the $(11\bar{2}0)$ surface, it is only when dissociation has occurred that a hydrogen-bonding network forms.

At high temperatures and low oxygen concentrations, we expect that a zinc-rich (oxygen deficient) surface will form at both surfaces considered. Although we carried out simulations at large defect coverages, we do observe that O defective surfaces can be thermodynamically stable (i.e., lie in the stability domain of ZnO). Although this maximum coverage (25%) is far larger than that required for the color change described in the Introduction to be observed, it suggests that the color change observed due to oxygen vacancies in the structure could be surface driven. This point is purely conjecture, however, since calculations with such large surface areas are still beyond the scope of the current computational resources.

Unlike previous work, where the entropic contribution to the free energy was assumed negligible, we have estimated this term using lattice dynamics based on an atomistic potential model. Our calculations, however, show that the contribution of this term is small, but at high temperatures and when two systems are similar in energy, as for associated and dissociated water on the surface, this small change in energy can be important.

Future work will move on to consider larger systems to determine the effect of coverage on the adsorption of water, oxygen vacancies, and other species on these systems. Furthermore, the good agreement between DFT and atomistic simulations suggests potential based methods can usefully be applied to ZnO.

Acknowledgment. We acknowledge the NERC funded e-minerals consortium and EPSRC grant GR/H0413 for funding and the National Grid Service and the HEFCE grant GR/S84415/01 for the provision of computer time.

References and Notes

(1) Mark, P.; Chang, S. C.; Creighton, W. F.; Lee, B. W. *Crit. Rev. Solid State Sci.* **1975**, *5*, 189.

(2) Duke, C. R.; Lubinsky, A. R.; Chang, S. C.; Lee, B. W.; Mark, P. *Phys. Rev. B* **1977**, *15*, 4865.

(3) Büchel, K. H.; Moretto, H. H.; Woditsch, P. *Industrial Inorganic Chemistry*, 2nd ed.; Wiley-VCH: Weinham, Germany, 2000.

(4) Greenwood, N. N. *Ionic crystals, lattice defects and nonstoichiometry*; Butterworth: London, UK, 1969.
(5) Göpel, W.; Lampe, U. *Phys. Rev. B* **1980**, *22*, 6447.
(6) Greenwood, N. N.; Earnshaw, A. *Chemistry of the Elements*, 2nd ed.; Butterworth-Heinmann: Oxford, UK, 1997.
(7) Duke, C. R.; Meyer, R. J.; Paton, A. *Phys. Rev. B* **1978**, *18*, 4225.
(8) Meyer, B.; Marx, D. *Phys. Rev. B* **2003**, *67*, 035403.
(9) Reuter, K.; Scheffler, M. *Phys. Rev. B* **2002**, *6503*, 035406.
(10) Wang, X. G.; Weiss, W.; Shaikhutdinov, S. K.; Ritter, M.; Petersen, M.; Wagner, F.; Schlogl, R.; Scheffler, M. *Phys. Rev. Lett.* **1998**, *81*, 1038.
(11) Batirev, I. G.; Alavi, A.; Finnis, M. W.; Deutsch, T. *Phys. Rev. Lett.* **1999**, *82*, 1510.
(12) Marmier, A.; Parker, S. C. *Phys. Rev. B* **2004**, *69*, 115409.
(13) Parker, S. C.; Kerisit, S.; Marmier, A.; Grigoleit, S.; Watson, G. W. *Faraday Discuss.* **2003**, *124*, 155.
(14) Meyer, B. *Phys. Rev. B* **2004**, *69*.
(15) Kresse, G.; Dulub, O.; Diebold, U. *Phys. Rev. B* **2003**, *68*, 245409.
(16) Meyer, B.; Marx, D.; Dulub, O.; Diebold, U.; Kunat, M.; Langenberg, D.; Woll, C. *Angew. Chem., Int. Ed.* **2004**, *43*, 6642.
(17) Kresse, G.; Furthmuller, J. *Comput. Mater. Sci.* **1996**, *6*, 15.
(18) Kresse, G.; Furthmuller, J. *Phys. Rev. B* **1996**, *54*, 11169.
(19) Kresse, G.; Hafner, J. *Phys. Rev. B* **1994**, *49*, 14251.
(20) Kresse, G.; Hafner, J. *Phys. Rev. B* **1993**, *47*, 558.
(21) Vanderbilt, D. *Phys. Rev. B* **1990**, *41*, 7892.
(22) Kresse, G.; Hafner, J. *J. Phys.-Condens. Matter* **1994**, *6*, 8245.
(23) Born, M.; Huang, K. *Dynamical theory of crystal lattices*; Oxford University Press: Oxford, UK, 1954.
(24) Binks, D. J.; Grimes, R. W. *J. Am. Ceram. Soc.* **1993**, *16*, 2370.
(25) Nyberg, M.; Nygren, M. A.; Pattersson, L. G. M.; Gay, D. H.; Rohl, A. L. *J. Phys. Chem.* **1996**, *100*, 9054.
(26) Wright, K.; Catlow, C. R. A. *Phys. Chem. Miner.* **1994**, *20*, 515.
(27) Parker, S. C.; Price, G. D. *Adv. Solid State Chem.* **1989**, *1*, 295.
(28) Tarento, R. J.; Harding, J. H. *J. Phys. C: Solid State Phys.* **1987**, *20*, L677.
(29) Taylor, M. B.; Barrera, G. D.; Allan, N. L.; Barron, T. H. K.; Mackrodt, W. C. *Faraday Discuss.* **1997**, *106*, 377.
(30) Cooke, D. J.; Parker, S. C.; Osguthorpe, D. J. *Phys. Rev. B* **2003**, *67*, 134306.
(31) Sawada, H.; Wang, R.; Sleight, A. W. *J. Solid State Chem.* **1996**, *122*, 148.
(32) Jaffe, J. E.; Harrison, N. M.; Hess, A. C. *Phys. Rev. B* **1993**, *49*, 11153.
(33) Schröer, P.; Kruger, P.; Pollmann, J. *Phys. Rev. B* **1993**, *47*, 6971.
(34) Wander, A.; Harrison, N. M. *Surf. Sci.* **2000**, *468*, L851.
(35) Whitmore, L.; Sokol, A. A.; Catlow, C. R. A. *Surf. Sci.* **2001**, *498*, 135.
(36) Duke, C. B.; Meyer, R. J.; Paton, A.; Mark, P. *Phys. Rev. B* **1978**, *18*, 4225.
(37) Filippetti, A.; Fiorentini, V.; Cappellini, G.; Bosin, A. *Phys. Rev. B* **1999**, *59*, 8026.
(38) Pollmann, J.; Krüger, P.; Rohlfing, M.; Sabisch, M.; Vogel, D. *Appl. Surf. Sci.* **1996**, *104*−*105*, 1.
(39) Fletcher, D. A.; McMeeking, R. F.; Parkin, D. J. *Chem. Inf. Comput. Sci.* **1996**, *36*, 746.
(40) Vannerberg, N. G. *Ark. Kemi* **1959**, *14*, 119.
(41) Odelius, M. *Phys. Rev. Lett.* **1999**, *82*, 3919.
(42) Giordano, L.; Goniakowski, J.; Suzanne, J. *Phys. Rev. Lett.* **1998**, *81*, 1271.
(43) Skinner, A. J.; Lafemina, J. P. *Phys. Rev. B* **1992**, *45*, 3557.